iScience, Volume *23*

Supplemental Information

Thioredoxin Interacting Protein Is Required for a Chronic Energy-Rich Diet to Promote Intestinal Fructose Absorption

Anu Shah, Sezin Dagdeviren, Jordan P. Lewandowski, Angela B. Schmider, Elisabeth M. Ricci-Blair, Niranjana Natarajan, Henna Hundal, Hye Lim Noh, Randall H. Friedline, Charles Vidoudez, Jason K. Kim, Amy J. Wagers, Roy J. Soberman, and Richard T. Lee

FIGURE S1: ERD increases acute fructose absorption in the presence of glucose or mannitol in the administering solution and ERD also raises ^{13}C -F1P levels. Related to Fig 1.

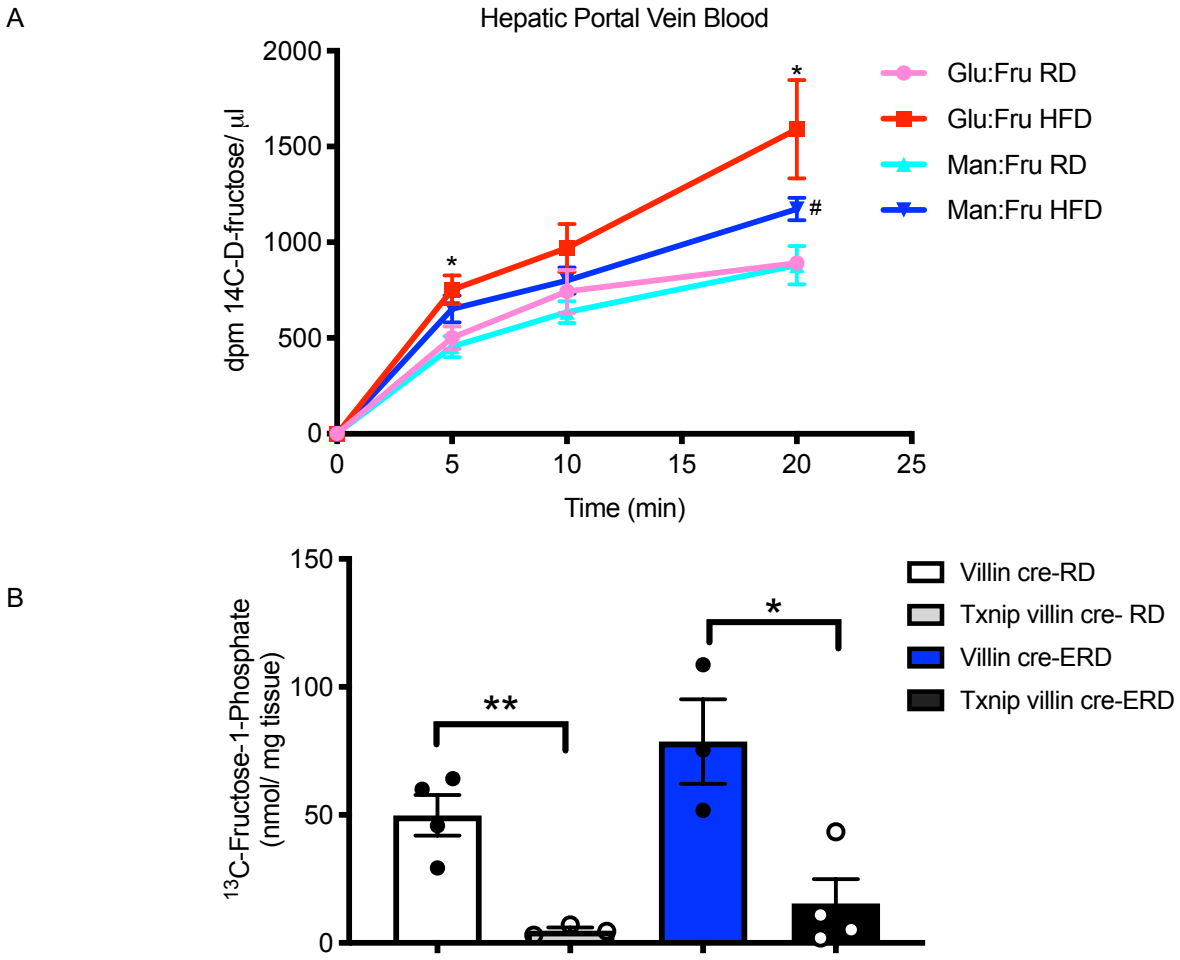

Figure S1. ERD increases acute fructose absorption in the presence of glucose or mannitol in the administering solution and ERD also raises ^{13}C -F1P levels. (A) C57BL/6J mice placed on RD or ERD for 8 weeks were subjected to a bolus oral gavage of radiolabeled fructose prepared in cold 1:1 mannitol: fructose (Man:Fru) or 1:1 glucose: fructose (Glu:Fru). Hepatic portal vein blood was obtained 0, 5, 10 or 20 min post gavage. Administration of radioactive fructose prepared in glucose solution elevated fructose absorption (i.e. 14C-fructose+ metabolites) significantly in the ERD-fed mice (*p<0.05 vs Glu:Fru RD) as early as 5 min post- gavage, unlike the mannitol administered group. However, at 20 min, fructose absorption increased significantly in the ERD groups regardless of glucose or mannitol mixed in the administering solution. (*p<0.05 vs Glu:Fru RD, # p<0.05 vs Man:Fru RD, n=6 (5 for time 0 min) /group for each time point). All values are mean± SEM and the statistical analyses were performed using an unpaired two-tailed *t*-test. (B) Txnip villin cre and villin cre mice placed on RD/ ERD for 16 weeks were given bolus intragastric gavage of ^{13}C-fructose to assess ^{13}C-F1P level in the jejuna after 20 min post gavage. All values are mean± SEM and the statistical analyses were performed using an unpaired two-tailed *t*-test where *p<0.05 vs and **p<0.01 (n=3-4 mice/ group).

FIGURE S2: Acute fructose absorption increases with chronic exposure to fructose in the diet. Related to Fig 1.

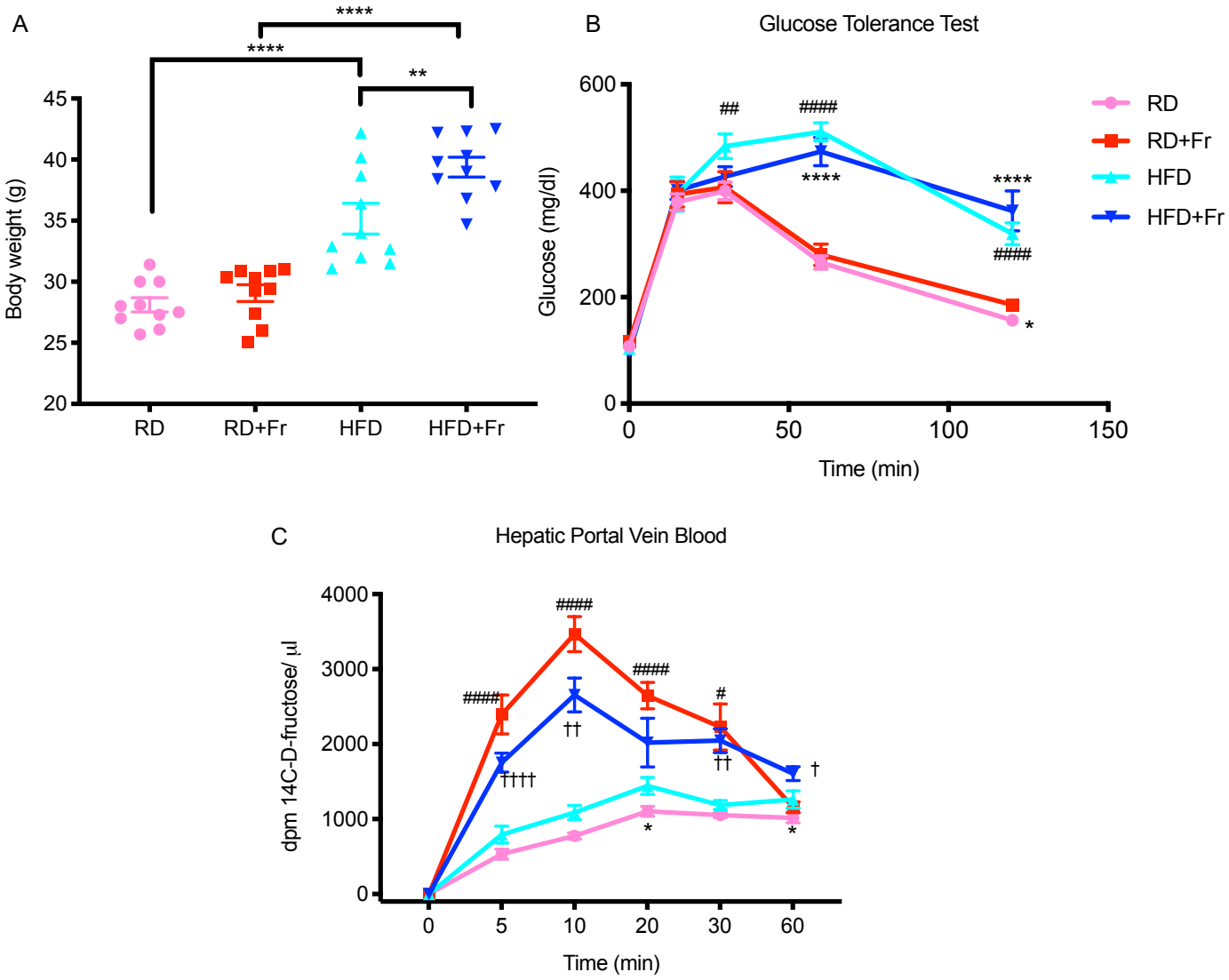

Figure S2. Acute fructose absorption increases with chronic exposure to fructose in the diet. A 4-week long study on RD or ERD-fed mice in the presence or absence of 30% fructose in water caused (A) a significant increase in body weight in mice fed a ERD as compared to ERD-fed mice with *ad libitum* access to water only (n=10 mice/ group, **p,0.01, ****p<0.0001). (B) Glucose tolerance tests illustrate that fructose in drinking water did not worsen glucose intolerance by ERD in 4 weeks (n=10 mice/ group, *p<0.05, ****p<0.0001 vs RD+Fr, ##p<0.01 and ####p<0.0001 vs RD). (C) Kinetics of fructose (i.e. 14C-fructose+ metabolites) absorption in hepatic portal vein blood assessed at 0, 5, 10, 20, 30, and 60 min post-oral gavage of radiolabeled fructose. For each time point, n=6 mice/ group were sacrificed to harvest tissues for analysis. Consistent with our previous study (Dotimas et al., 2016), fructose absorption peaked at 20-min after radiolabeled fructose gavage in mice that did not receive fructose in drinking water. However, mice that received fructose in drinking water had a peak portal vein absorption at 10 minutes, in the presence or absence of ERD. All values are mean± SEM, and the statistical analysis was performed using an unpaired two-tailed *t*-test; n=6 for each group at each time-point, #p<0.05 and ####p<0.0001 vs RD; †p<0.05, ††p<0.01, †††† p<0.0001 vs ERD.

FIGURE S3: Intestinal Txnip does not alter tissue responsiveness to nitric oxide. Related to Fig 3.

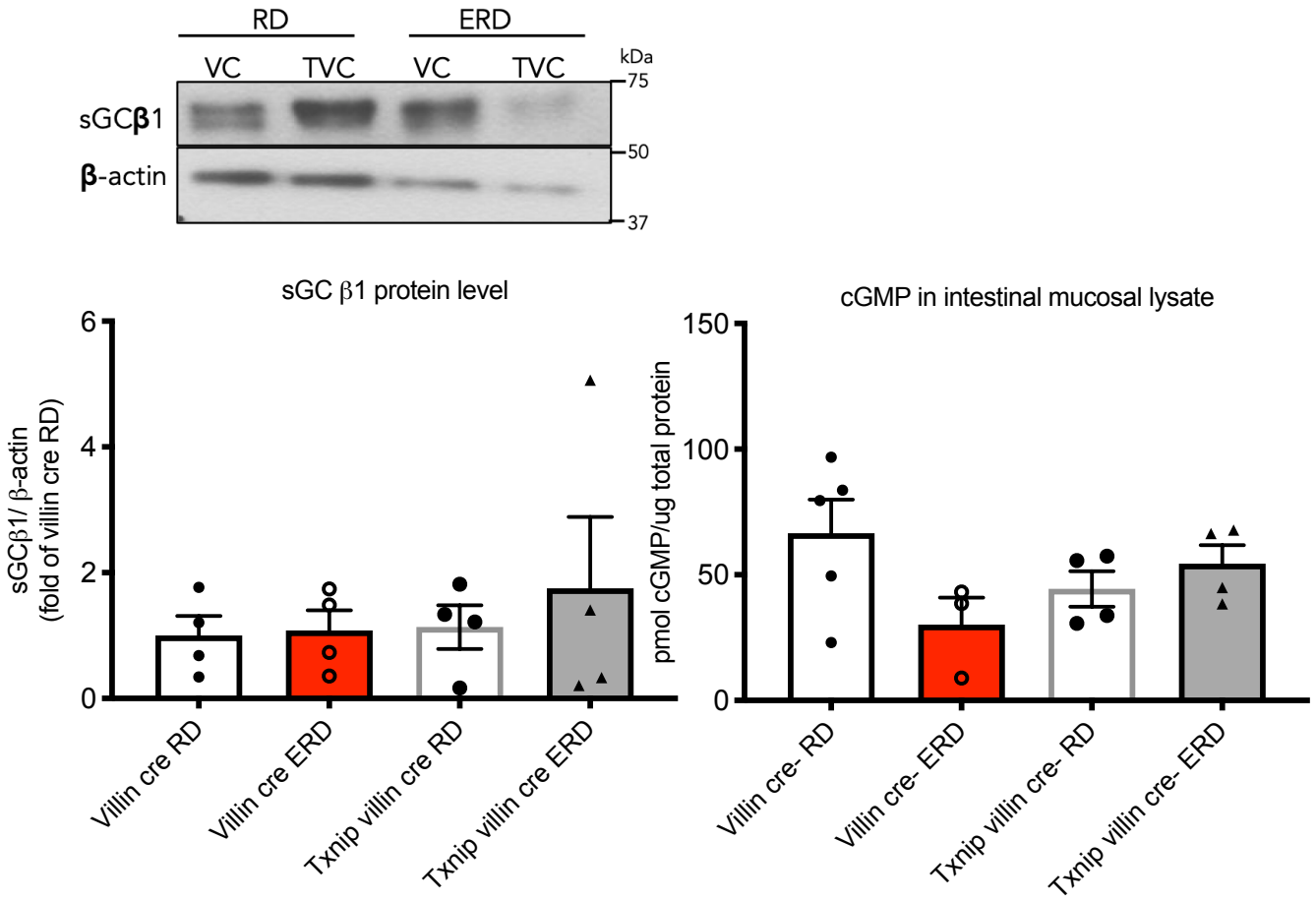

Figure S3. Intestinal Txnip does not alter tissue responsiveness to nitric oxide. Intestinal mucosal lysates from villin cre and Txnip villin cre mice placed on a RD were not significantly different in soluble guanylate cyclase β1(sGCβ1) protein expression (left panel, n=4) or its the activation (via cGMP activity) (right panel, n=3-5) after ERD feeding. Moreover, intestinal Txnip expression did not affect these parameters. All the values are mean± SEM and the statistical analyses were performed using an unpaired two-tailed *t*-test, with no significant differences found.

FIGURE S4: Chromatin immunoprecipitation (ChIP) on intestinal tissue from mice with H2O (n=2) and mice with fructose (n=1) for ChREBP, H3K4me3, and IgG followed by quantitative PCR (QPCR) to assay enrichment at three different loci. Related to Fig 3.

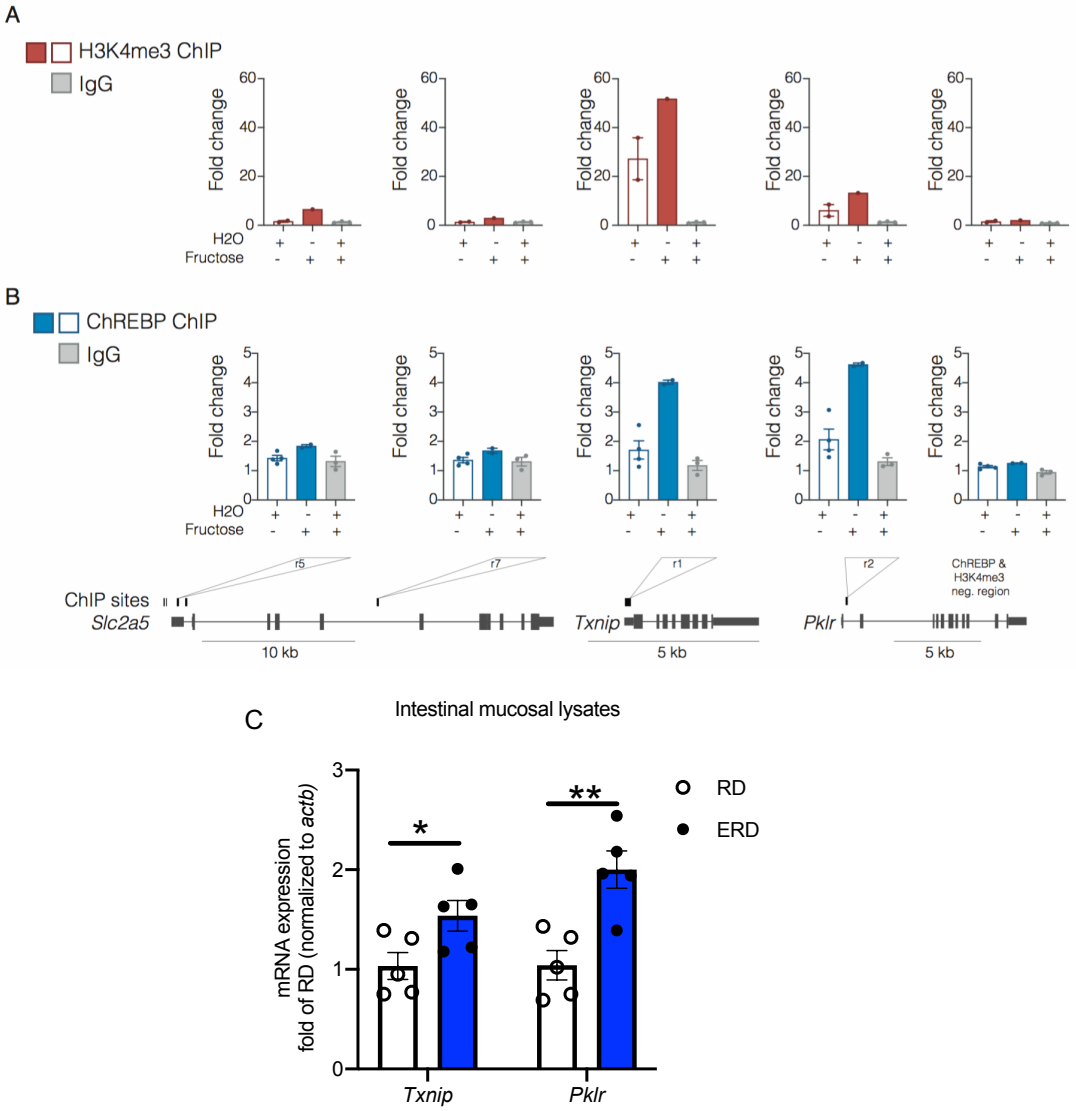

Figure S4. Chromatin immunoprecipitation (ChIP) on intestinal tissue from mice with H2O (n=2) and mice with fructose (n=1) for ChREBP, H3K4me3, and IgG followed by quantitative PCR (QPCR) to assay enrichment at three different loci. (A) H3K4me3 ChIP in H2O treated (n=2 ChIPs), fructose treated (n=1 ChIP), and IgG samples (n=3 ChIPs). Enrichment assayed at *Slc2a5*, *Txnip*, and *Pklr*. (B) ChREBP ChIP in H2O treated (n=4 ChIPs), fructose treated (n=2 ChIPs), and IgG samples (n=3 ChIPs). *Slc2a5* promoter and gene body showing two different ChIP regions assayed r5 and r7, which is previously identified ChREBP binding region (Kim et al., 2017). r5 is in proximity to two previously reported ChREBP binding sites (Oh et al., 2018). Positive control regions for ChREBP at the *Txnip* promoter (r1) (Poungvarin et al., 2015) and Pyruvate kinase L/R (Pklr) promoter (r2) (Kim et al., 2017). And a ChREBP negative control region at the *Pklr* promoter (Kim et al., 2017). The mean is shown and the error bars represent the standard error of the mean. Genomic loci shown are from University of Santa Cruz Genome Browser (UCSC), mm10. (C) Relative gene expression of intestinal *Txnip* and *Pklr* after mice were fed a RD or ERD. All values are mean± SEM, and the statistical analysis was performed using an unpaired two-tailed *t*-test; n=5, $^{*}p<0.05$ and $^{**}p<0.01$ vs RD.

FIGURE S5: Cluster maps for Txnip with Glut5 and Txnip with Rab11a . Related to Fig 4.

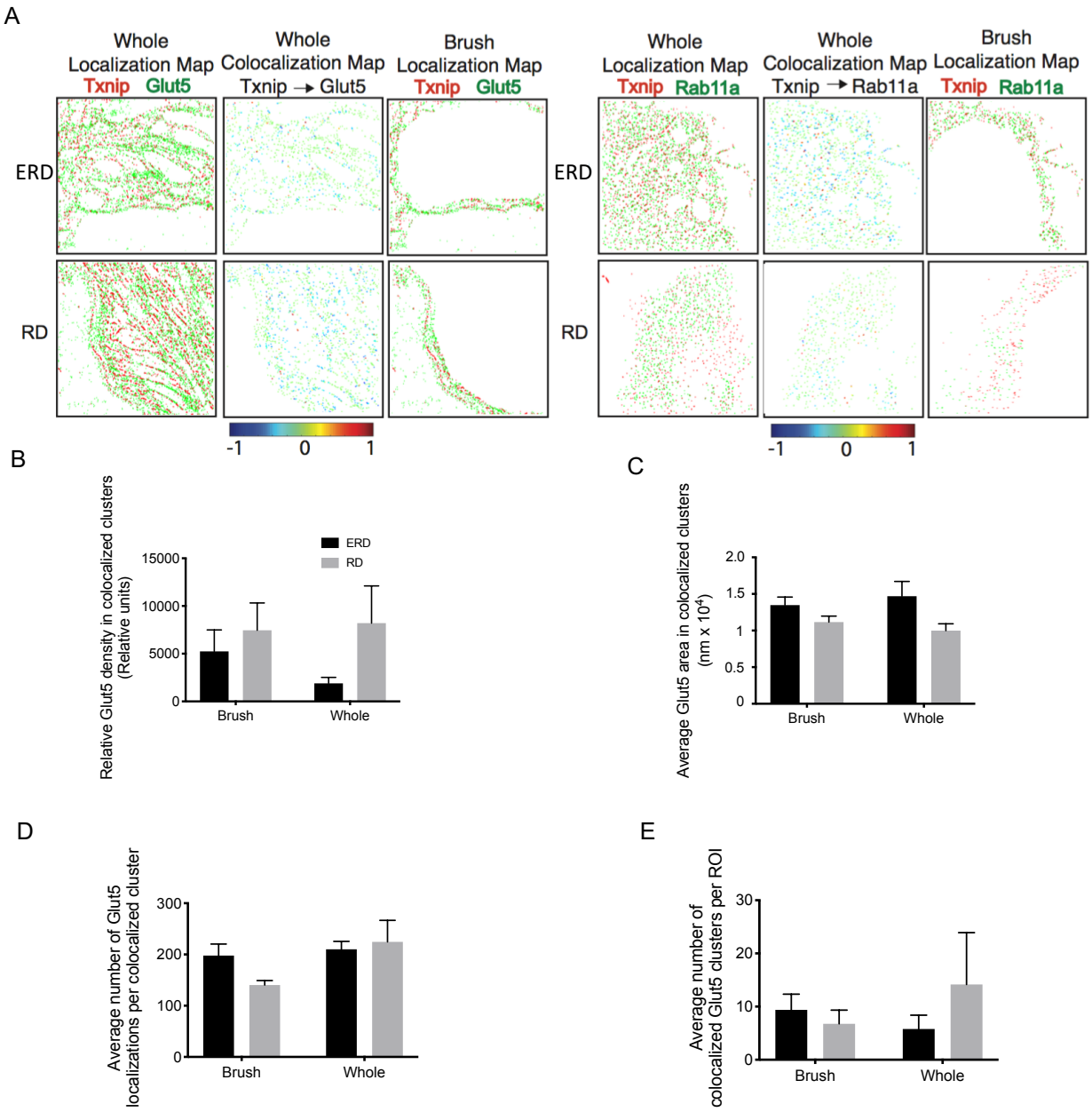

Figure S5. Cluster maps for Txnip with Glut5 and Txnip with Rab11a. (A) Localization maps for Txnip (red) and Glut5 or Rab11 (green) encompassing apical to basolateral brush border (whole) or only apical brush border (brush). Maps for Txnip relative to Glut5 left panels. Txnip localizations are pseudocolor-coded according to their degree of colocalization (DoC) scores (score bar at the bottom). Right panels show localization maps for Txnip and Rab11a. Clusters were defined as having ≥ 10 localizations with a DoC score of ≥ 0.4 for figures B-E. Glut5 cluster properties: (B) relative density; (C) average area; (D) average number of localizations; and (E) average number of cluster per ROI. The relative density of clusters was calculated by dividing the local density within 20 nm of each localization by the average density of the cluster, a measure of the local concentration maxima within the cluster. Statistical significance was assessed by two-way ANOVA with multiple comparisons and a Tukey post-test with significance indicated by *p<0.05. Bars show mean ± SEM from 5-13 ROIs over 3 separate mice. Scale bar represents 10 μM.

Table S1. Metabolic profile of RD or ERD-fed mice. Related to Fig 1.

	4-weeks diet		16-weeks diet	
	RD (n=7)	ERD (n=7)	RD (n=14-16)	ERD (n=14-16)
Body weight (g)	28.9±0.2	35.7±1.5**	31.4±0.5	42.7±1.0***
Fasting blood glucose (mg/dL)	117.3±3.8	108.0±9.3	109.2±10.4	115.1±5.7
AUC- Glucose tolerance test (a.u.)	31707.5± 1040.8	51019.3± 2116.2***	36596.0± 989.6	60884.5± 1583.6***

Table S1. Metabolic profile of RD or ERD-fed mice. Results are expressed as mean ± SEM (n=7/ group (4 weeks-diet) and n=14-17/group (16 weeks-diet). P-values were calculated using an unpaired student's *t*-test for body weight and fasting glucose, and one-way ANOVA followed by Bonferroni's *post-hoc* test was employed for the AUC from Glucose tolerance test (GTT). **p<0.05 and ***p<0.0001 vs their own RD diet control.

Table S2. Metabolic profile of Txnip villin cre and Villin cre mice. Related to Fig 2.

4-weeks diet	Villin cre		Txnip villin cre	
	RD (n=5)	ERD (n=5)	RD (n=5)	ERD (n=4)
Body weight (g)	25.8±0.8	33.9±1.9**	27.2±0.1	35.9±1.9*
Fasting blood glucose (mg/dL)	116.0±9.0	132.0±5.5	117.2±6.5	132.5±7.7
AUC- Glucose tolerance test (a.u.)	23794.5± 722.4	42777.0± 1639.0***	24030.0± 766.6	34346.3± 1058.3***,$^{+++}$
16-weeks diet	Villin cre		Txnip villin cre	
	RD (n=5)	ERD (n=5)	RD (n=5)	ERD (n=3)
Body weight (g)	28.0±0.9	48.5±1.3***	30.8±1.1	51.2±0.8***
Fasting blood glucose (mg/dL)	104.4±5.9	114.4±7.3	117.4±5.4	122.0±17.0
AUC- Glucose tolerance test (a.u.)	30343.5± 939.0	53818.5± 2483.6***	23788.5± 640.2	55617.5± 3188.1***

Table S2. Metabolic profile of Txnip villin cre and Villin cre mice. Results are expressed as mean ± SEM (n=4-5/ group (4 weeks-diet) and n=3-5/ group (16 weeks-diet). P-values were calculated using an unpaired student's *t*-test for body weight and fasting glucose, and one-way ANOVA followed by Bonferroni's *post-hoc* test was employed for the AUC from Glucose tolerance test (GTT). *p<0.05, **p<0.01, and ***p<0.001 vs their own regular diet control; $^{+++}$p<0.001 vs villin cre ERD.

TRANSPARENT METHODS

Animal care and diets

All experiments were conducted in accordance with the Guidelines for the Use and Care of Laboratory Animals and approved by the Harvard University Institutional Animal Care and Use Committee (protocol number 16-05-271 and 16-05-272). All the mice were housed at controlled temperature (20-21°C) on a 12h light/dark cycle. Txnip knockout (KO) mice were generated in our lab and C57Bl/6J was used as Txnip wildtype (WT) control. For fructose absorption studies, C57Bl/6J male mice, subjected to either 4-weeks or 16-weeks of regular (RD) or energy rich diet (ERD), were obtained from JAX. Txnip villin cre (Txnip $^{fl/fl}$ villin cre $^{+/-}$) mice were generated by breeding Txnip $^{fl/fl}$ mice (Yoshioka et al., 2007), generated in our lab, with villin cre mice (Vil-Cre 1000, JAX). Age-matching villin cre (Txnip$^{+/+}$ cre $^{+/-}$) mice were used as controls. 7-9 weeks old mice were randomly subjected to RD (Prolab®IsoPro® RMH 3000, 5P75/ 5P76) or ERD (60% kcal HFD, ResearchDiets Inc., D12492), and provided free access to water. In the experiments where mice were supplemented with fructose solution to their diet, 30% fructose solution in drinking water was used.

The number of mice required for the study was determined by using the sample size calculations from the IACUC at Boston University (https://www.bu.edu/researchsupport/compliance), and an alpha of 0.05 and statistical power of 90% were used as parameters to estimate the appropriate sample size. All the experiments were performed as independent biological replications (for example: n=3 means three mice), except for the qPCR and ChIP assays that have both biological and technical replications. Moreover, the inclusion and exclusion of data was verified by the Graphpad Outlier calculator (https://www.graphpad.com/quickcalcs/Grubbs1.cfm) where alpha=0.05.

In vivo bio-distribution assay with radiolabeled fructose

Intestinal fructose uptake and bio-distribution was assessed as previously described (Dotimas et al., 2016) but with a slight modification. Briefly, 20 minutes after the intragastric administration of 2 µCi [14C(U)]-D-fructose (Moravek Inc.) in 200µl 30% of non-radioactive fructose/ mannitol, blood samples were collected from tail and portal veins and tissues were harvested. We used mannitol instead of glucose in the administering solution in order to avoid effects of glucose on fructose uptake as shown in Supplemental Figure S1A**.** $Ba(OH)_2$ and ZnSO4 were used to precipitate proteins in plasma, and the supernatants were counted using Ultima Gold Scintillation fluid (PerkinElmer). Similarly, 100-150mg of tissues were homogenized using 10X volume of water and boiled for 10 min at 100°C. The samples were then centrifuged and 500µl of clear supernatant was added to 5 ml scintillation fluid. Pre-weighed intestinal were dissolved in 1ml soluene (Soluene®-350, PerkinElmer) at 55°C for 4h before adding them to 5 ml scintillation fluid. Radioactivity in tissues was measured in the Beckman Coulter LS 6500 Liquid Scintillation Counter.

Glucose tolerance test

Glucose tolerance test (GTT) was performed after overnight fasting. After obtaining body weight and basal blood glucose reading from a tail clip, mice were administered a bolus glucose (2g/kg body weight) intraperitoneally. Blood glucose values were then obtained at 15, 30, 60, 90, and 120 minutes using a Bayer Contour Blood Glucometer.

Metabolic studies

Metabolic changes were measured at the National Mouse Metabolic Phenotyping Center (MMPC) at the University of Massachusetts Medical School. Briefly, mice were individually placed in metabolic cages (TSE-Systems Inc., Bad Homburg, Germany) for 3 days to non-invasively assess their indirect calorimetry and energy balance parameters, including physical activity, food/ water intake, respiratory exchange ratio, and energy expenditure. Whole body fat and lean fat were non-invasively assessed in awake mice via proton magnetic resonance spectroscopy (^{1}H-MRS) (Echo Medical Systems, Houston, TX). Liver triglycerides, plasma cholesterol, and HDL/ LDL were assessed by the Analytical Core of UMass MMPC.

Immunoblotting

Villi were extracted from the small intestine using the procedure as previously described (Booth and O'Shea, 2002). Immunoblotting on homogenized jejunal samples and villi were performed as described

previously (Shah et al., 2015). For primary antibodies, anti-Txnip (MBL) and anti-Glut5 (EMD Millipore, 07-1406) were used at 1:1000 dilution, and β-actin (Santa Cruz) at 1:10000.

Quantitative PCR analysis

Frozen tissues were homogenized in TRIZOL reagent (Invitrogen) to extract RNA. cDNA synthesis on 1µg RNA was performed using the High Capacity cDNA Reverse Transcription kit (Applied Biosystems). The cDNA was then used for real-time PCR analysis using the Taqman Gene Expression System, where the following mouse-specific primers were used: *Txnip* (Mm00452393_m1), *Slc2a5* (Mm00600311_m1), *Pklr* (Mm00443090_m1), and the housekeeping gene, *Actb* (Mm02619580_g1). Relative gene expression was calculated as mentioned before (Dotimas et al., 2016).

Extraction and fructose uptake in intestinal organoids

Intestinal organoids from Txnip WT and KO mice were extracted and maintained according to the protocol previously described by Zietek et al., 2015. Fructose uptake assay was performed on differentiated organoids (proliferated/ budded organoids), from days 5-7, also following the protocol from the same article.

Histology, N-STORM and co-localization analysis

Cryostat sections of jejuna (1-µm) were incubated overnight in 1:100 dilution of primary antibodies: anti-Txnip (MBL), anti-Glut5 (EMD Millipore, 07-1406) and anti-RAB11A (US Biological, R0009) in PBS containing 0.2 % skim milk and 1% BSA. Tissues were then incubated for 1h at room temperature with 3µg/ml secondary antibodies that were made in house to achieve a near ratio of 1:1, antibody: fluorophore, respectively. After nuclei staining with DAPI (1:1000), tissues were fixed with 4% PFA followed by visualization and analysis via Stochastic Optical Reconstruction Microscopy (N-STORM). Briefly, the imaging buffer containing 100 mM 2-mercaptoethanolamine (MEA) and 1% (v/v) GLOX was used to promote photoswitching and reduce photobleaching. An inverted Nikon Ti2 Eclipse STORM 5.0 system with Perfect Focus focal plane lock was used for image acquisition. This system contains a NSTORM quadband filter, and 405, 488, 561, and 647 nm lasers and was equipped with an HP APO TIRF AC 100x/1.49 NA oil objective and ORCA-Flash4.0 SCI CMOS PLUS camera (Hamamatsu Photonics). 15,000 frames for each dye were collected at 30 ms exposure time in continuous mode. Localizations were identified with NIS Elements 5.0 (Nikon Instruments) and exported as tab-delimited text files.
To produce reporter antibodies for dSTORM, donkey anti-rabbit and donkey anti-mouse affinity purified secondary antibodies (H+L chains) (Jackson Laboratory) were conjugated to Cy3B (GE Healthcare) or AF647 dyes, both with carboxylic acid succinimidyl ester moieties. For the conjugation reactions, 240 µg of the secondary antibody was reacted with 6 µg of dye in 56 mM carbonic buffer for 2 hours at room temperature. After the reactions, the antibodies were separated from unconjugated dye by gravity filtration through Sephadex G-25 DNA grade size exclusion columns (GE Healthcare) by visual detection. Antibody and dye concentrations were determined using a NanoDrop spectrometer (Thermo Fisher) to record absorbance at 280 nm and at the dye absorbance peak. Antibody concentration was calculated by subtracting the contribution of each dye to absorbance at 280 nm using correction factors provided by the dye manufacturers (Cy3B: 0.09, AF647: 0.03) and the molar extinction coefficient of the antibody (210,000). The final ratio for the donkey-anti-rabbit: Cy3B was 1:2 with antibody concentration of 151 µg/µL. The final ratio for the donkey-anti-mouse:AF647 was 1:5 with antibody concentration of 200 µg/µL.

Clus-DoC analysis of single molecule localizations

We employed Clus-DoC (Pageon et al., 2016), which quantifies colocalization of individual proteins and molecules (localizations) and cluster properties (Schmider, 2019) to analyze dSTORM localization Clus-DoC allows for the user to define the number and DoC threshold.

In brief, co-localization between two proteins (localizations/molecules) is analyzed at the single-molecule level. This coordinate-based co-localization method uses algorithms that detect and save coordinates of single molecules. The spatial distribution surrounding localizations from both proteins of interest is compared to a single point. The density gradients of both proteins are generated. Next, the two distributions (densities) are compared by calculating a rank correlation coefficient where each molecule is assigned a

degree of co-localization (DoC) score ranging from -1 (segregated) to 0 (non-co-localized) to +1 (perfectly co-localized). Finally, because majority of the DoC scores where >0.4 with a peak at 1 (high col-localization), a threshold of 0.4 was used to distinguish co-localized from non-co-localized localizations.

Fructose Isotope gavage and sample collection
Animals were starved for 5h before administering them with 1:1 mixture of unlabeled mannitol and labeled [U-^{13}C]-fructose (Cambridge Isotope Labs, CLM-1553-PK), 2g/kg each via intragastric gavage. Mice were euthanized 20 min later and their tissues were harvested and frozen in -70°C until extraction.

Metabolite extraction and LC-MS
Tissues were extracted in guidance of the Harvard Small Molecule Mass Spectrometry facility. Briefly, tissues were homogenized with a homogenizer in HPLC grade cold methanol (4°C) before adding HPLC grade chloroform and LC/MS grade water. After centrifugation, the aqueous phases were isolated, dried using nitrogen evaporator and then submitted to the Mass Spectrometry facility. LC-MS analysis was performed using a Thermo Q- Exactive Plus Hybrid Quadrupole- Orbitrap mass spectrometer, coupled with a Thermo UltiMate 3000 LC and a Millipore zic-pHILIC column.

Immunostaining and Confocal Microscopy

Cryostat sections (1-μm) from jejuna of Txnip WT and KO mice fed with either RD or ERD for 1 month were incubated with 1:100 dilution of anti-Glut5 (EMD) overnight in 4°C. Incubation with secondary antibody (1:500, goat anti-rabbit Alexa Flour 488 from Invitrogen) along with 1:1000 Hoechst 33342 was done for 1h at RT. Confocal imaging to assess expression of Glut5 in the tissues was carried out using Zeiss LSM 880 with Airyscan detector (GaAsP-PMT super-resolution detector) at the Harvard Center for Biological Imaging. The Airyscan detector (Huff, 2015) was used to get a high-resolution image of Glut 5 expression in enterocytes and the brush-border membrane using a 63X oil immersion objective.

Chromatin immunoprecipitation (ChIP)
ChIP experiments were performed using the iDeal ChIP-qPCR kit (Diagenode, C01010180) according to the manufacturer's instructions. We performed two independent ChREBP ChIP experiments. We used C57Bl/6J male mice that were fed a RD (n=2) or ERD (n=2) for 15 weeks. We then extracted approximately 200 mg of mucosal layer from the jejuna and crosslinked the tissue in 1% methanol-free formaldehyde solution (Thermo Scientific, 28906) for 20 min at room temperature with gentle agitation. The isolated chromatin was sheared with a Bioruptor (Diagenode) using 18 cycles of 30 s 'on' and 30 s 'off'. Fresh chromatin was used for multiple individual ChIP reactions. We added either 2μg of ChREBP (Abcam, ab92809), 2 μg of IgG (Diagenode, K02921003), or 2μg of H3K4me3 antibodies (Diagenode, K02921004). 1% of the sheared chromatin was retained for the input control. The occupancy of ChREBP and H3K4me3 at the promoters of *Slc2a5*, *Txnip*, and *Pklr* was assessed by real-time qPCR on a ViiA7 Real-Time PCR System (ABI) using FastStart Universal SYBR Green Master (Rox) (ABI, 4913914001) with the following cycling parameters: 95°C for 10min, followed by 40 cycles of 95°C for 10 seconds and 60°C for 30 seconds. The enrichment values were determined by the ΔΔCt method of normalized IP over normalized input using the baseline primer pairs F-baseline and R-baseline (Vokes et al., 2007), where ΔΔC(t) = ΔC(t)ChIP - ΔC(t)Input; ΔC(t)ChIP = C(t)experimental primer - C(t) baseline primer in the ChIP sample and ΔC(t)Input = C(t)experimental primer – C(t) baseline primer in the input sample. We used the following primers for qPCR:
F-r1: GGGGTTTCCAGAGTTTCTCC; R-r1: CTCCGTAAAGTCAGGGCTTG (Poungvarin et al., 2015)

F-r2: TTTGATCCAGGCTCTGCAGAC; R-r2: TCTTGCCAATGGAAGCCTTG (Kim et al., 2017)

F-r3: GAT TTC CTG CCG CAT TCA GA; R-r3: TTT TCAGAC CTC CCA GAT GGA (Oh et al., 2018)

F-r4: TCC ATC CAC ACA CTTTCA AAC; R-r4: CAA GCC ACG GCC AAC AG (Oh et al., 2018)

F-r5: AGTTGAAGAGCCACCGTGTT; R-r5: AGTGTAGATCCGCTCGGGTA

F-r6: AGCACAGGCAATCCGTACTC; R-r6: GCCTAGTGTTTCCCACCACA
F-r7: GGGACTGAGAAACATCCGGG; R-r7: TGTTGCCCAAGGTGCTGATA (Kim et al., 2017)

F-neg: TGGACATTTGACTCCAGAGC; R-neg: AACATGGAGAAGAAGGCAGTG (Kim et al., 2017)

F-baseline: CTGGCCTCCATACACACATA; R-baseline: AGTCAGCAGGATCCACACTT (Vokes et al., 2007)

ChREBP ChIP response to a classical stimuli (fructose) was assessed in C57Bl/6J mice following the protocol described by Kim *et al*. (Kim et al., 2017).

Statistical analyses

Data are presented as mean ± SEM, unless otherwise stated. P-values were calculated using an unpaired student's *t*-test since we were specifically comparing 2 groups at a time (such as comparison between the fructose absorption due to two different diets on the same strain of mice, or difference in the absorption by two different strains of mice placed on same diet). To calculate the statistical significance of AUC for glucose tolerance test (GTT), one-way ANOVA followed by Bonferroni *post hoc* method was used (Graphpad Prism, version 7.0). Two-way ANOVA with multiple comparisons and a Tukey post-test was employed for the colocalization studies via STORM, where significance was indicated by *$p<0.05$.

SUPPLEMENTAL REFERENCES

Booth, C., and O'Shea, J.A. (2002). Isolation and Culture of Intestinal Epithelial Cells. In Culture of specialized cells, R.I. Freshney, and M.G. Freshney, eds. (New York: Wiley-Liss), pp. xv, 461 p.

Dotimas, J.R., Lee, A.W., Schmider, A.B., Carroll, S.H., Shah, A., Bilen, J., Elliott, K.R., Myers, R.B., Soberman, R.J., Yoshioka, J.*, et al.* (2016). Diabetes regulates fructose absorption through thioredoxin-interacting protein. Elife *5*.

Huff, J. (2015). The Airyscan detector from ZEISS: confocal imaging with improved signal-to-noise ratio and super-resolution. Nature Methods *12*, i-ii.

Kim, M., Astapova, II, Flier, S.N., Hannou, S.A., Doridot, L., Sargsyan, A., Kou, H.H., Fowler, A.J., Liang, G., and Herman, M.A. (2017). Intestinal, but not hepatic, ChREBP is required for fructose tolerance. JCI Insight *2*.

Oh, A.R., Sohn, S., Lee, J., Park, J.M., Nam, K.T., Hahm, K.B., Kim, Y.B., Lee, H.J., and Cha, J.Y. (2018). ChREBP deficiency leads to diarrhea-predominant irritable bowel syndrome. Metabolism *85*, 286-297.

Pageon, S.V., Nicovich, P.R., Mollazade, M., Tabarin, T., and Gaus, K. (2016). Clus-DoC: a combined cluster detection and colocalization analysis for single-molecule localization microscopy data. Mol Biol Cell *27*, 3627-3636.

Poungvarin, N., Chang, B., Imamura, M., Chen, J., Moolsuwan, K., Sae-Lee, C., Li, W., and Chan, L. (2015). Genome-Wide Analysis of ChREBP Binding Sites on Male Mouse Liver and White Adipose Chromatin. Endocrinology *156*, 1982-1994.

Schmider, A.B., Vaught M., Bauer, N.C., Elliott, H.L., Godin, M.D., Ellis, G.E., Nigrovic, P.A. and Soberman, R.J. (2019). The organization of leukotriene biosynthesis on the nuclear envelope revealed by single molecule localization microscopy and computational analyses. PlosOne *Accepted and in press*.

Shah, A., Xia, L., Masson, E.A., Gui, C., Momen, A., Shikatani, E.A., Husain, M., Quaggin, S., John, R., and Fantus, I.G. (2015). Thioredoxin-Interacting Protein Deficiency Protects against Diabetic Nephropathy. J Am Soc Nephrol *26*, 2963-2977.

Vokes, S.A., Ji, H., McCuine, S., Tenzen, T., Giles, S., Zhong, S., Longabaugh, W.J., Davidson, E.H., Wong, W.H., and McMahon, A.P. (2007). Genomic characterization of Gli-activator targets in sonic hedgehog-mediated neural patterning. Development *134*, 1977-1989.

Yoshioka, J., Imahashi, K., Gabel, S.A., Chutkow, W.A., Burds, A.A., Gannon, J., Schulze, P.C., MacGillivray, C., London, R.E., Murphy, E.*, et al.* (2007). Targeted deletion of thioredoxin-interacting protein regulates cardiac dysfunction in response to pressure overload. Circ Res *101*, 1328-1338.